Figure Supplement

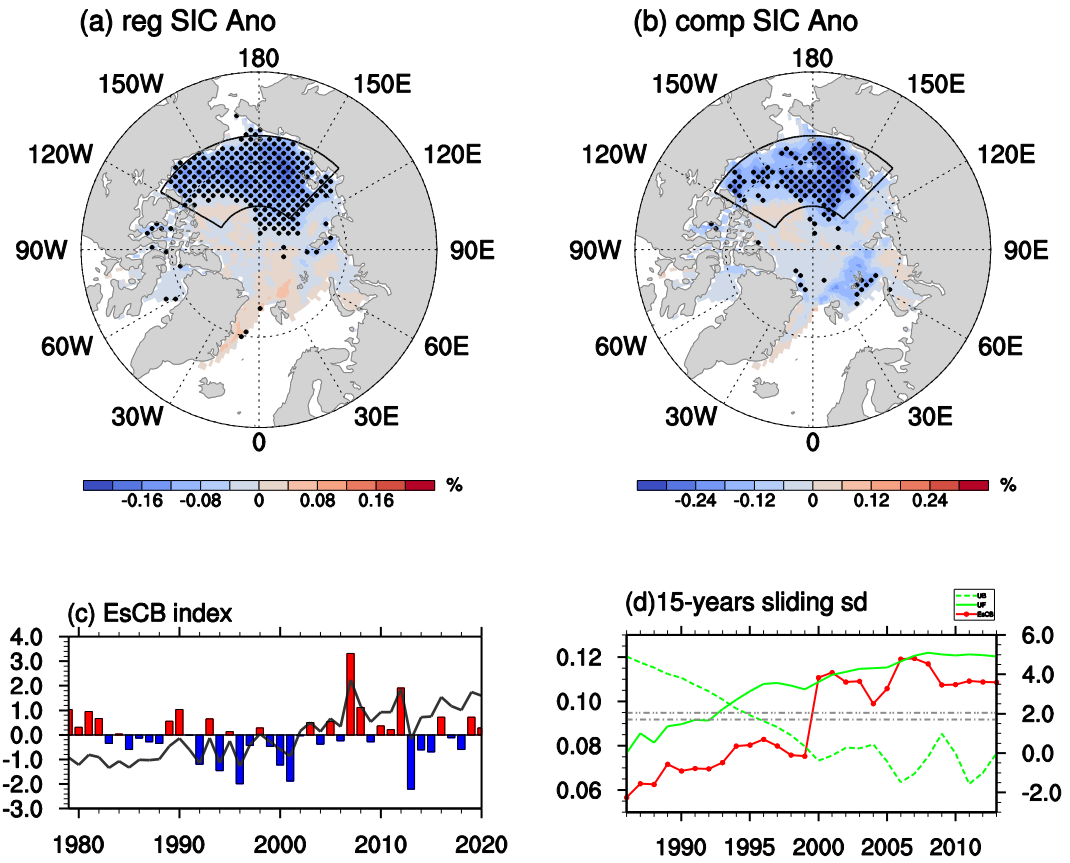

Figure S1 (a) Regressed SO sea ice concentration (SIC) anomalies (Shading, unit: %) on normalized SO detrended EsCB index, (b) Composite detrended SIC anomalies (Shading, unit: %) for six low EsCB sea ice years (1979, 1981, 1990, 2007, 2008, 2012), (c) the original EsCB index (black line) and its detrended component (bar chart), and (d) 15-year sliding standard deviation (red dot line) of autumn EsCB index and associated Mann-Kendall (M-K) test (dashed and solid green line). Black dots in (a) and (b) indicates 90% confidence level. Gray double (single) dotted line in (c) indicates 95% (90%) confidence level.

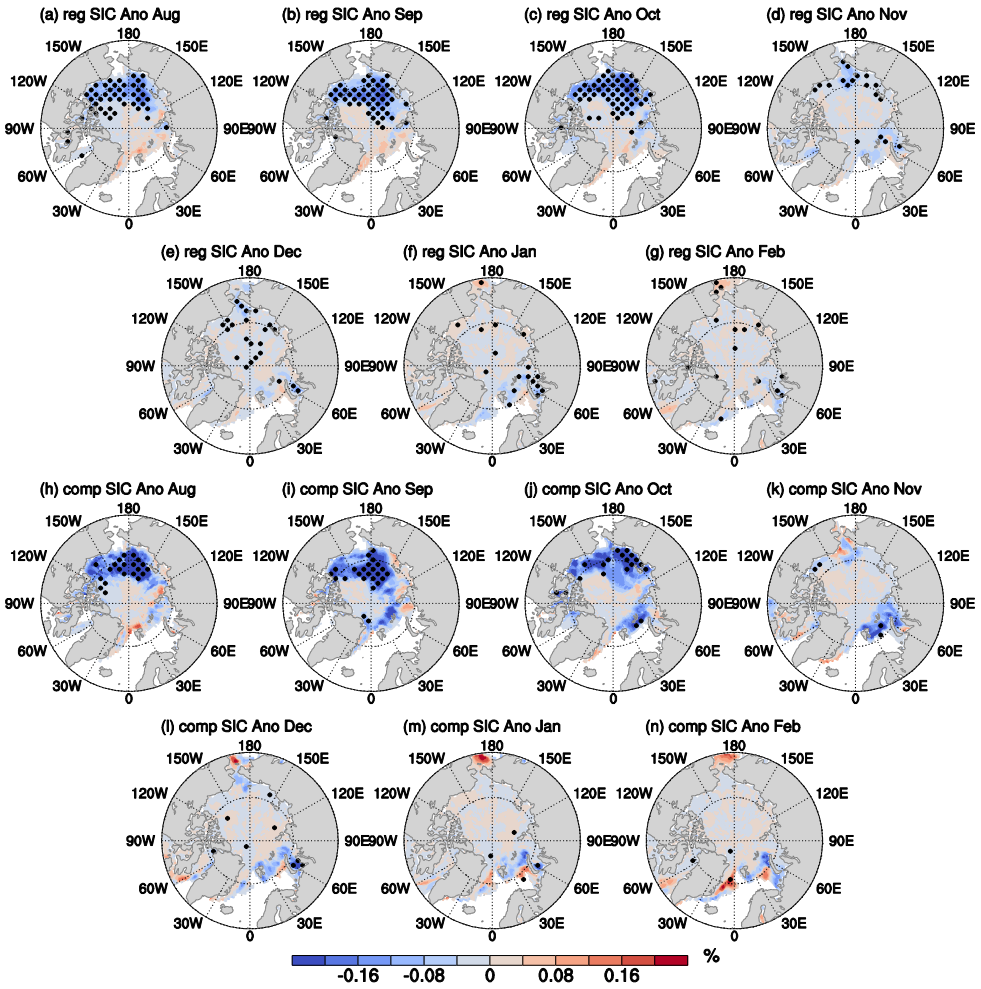

Figure S2 (a) Regressed sea ice concentration (SIC) anomalies (Shading, unit: %) on normalized autumn detrended EsCB index from (a) August to (g) February. (h) - (n) same as (a) - (g), but for composite detrended SIC anomalies (Shading, unit: %) for six low EsCB sea ice years (1979, 1981, 1990, 2007, 2008, 2012). Black dots in (a) and (b) indicates 90% confidence level.

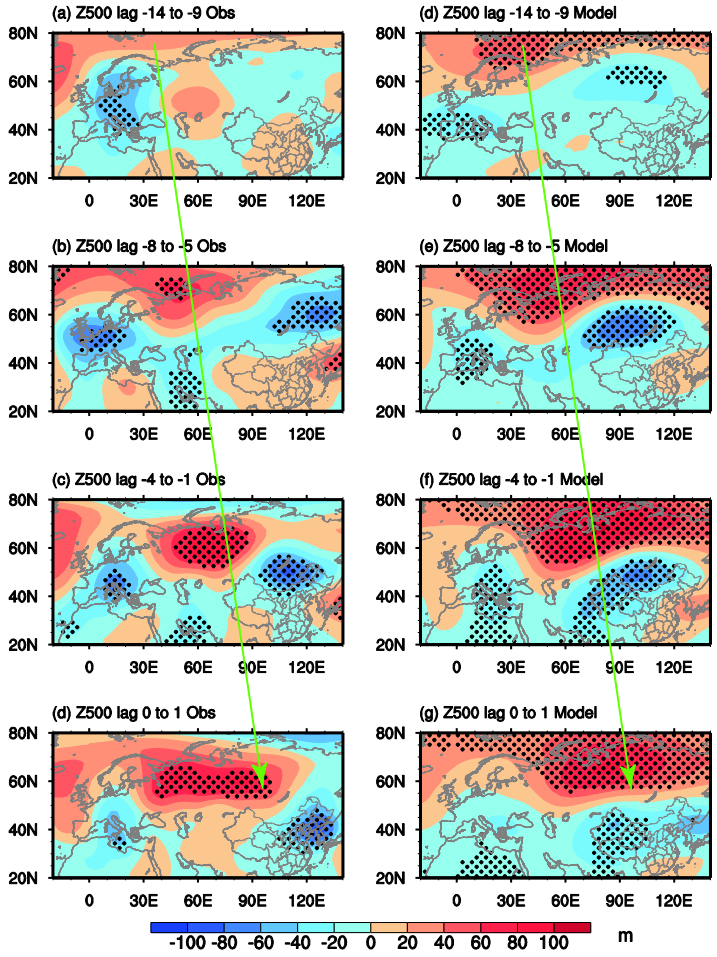

Figure S3 Composite evolution of detrended geopotential height anomalies (shading, unit: m) at 500 hPa in (a) day -14 ~ -9, (b) day -8 ~ -5, (c) day -4 ~ -1 and (d) day 0 ~ 1 for 12 extreme low temperature events over central-western China during six low EsCB sea ice years. (g) – (l) same as (a) - (f), but for simulated results with 185 extreme low temperature events in 100 members. Black dots contours indicate 90% confidence level. The interval of contour is 20 m. Green line arrow indicates the downstream development of the Northern European anticyclonic anomaly.

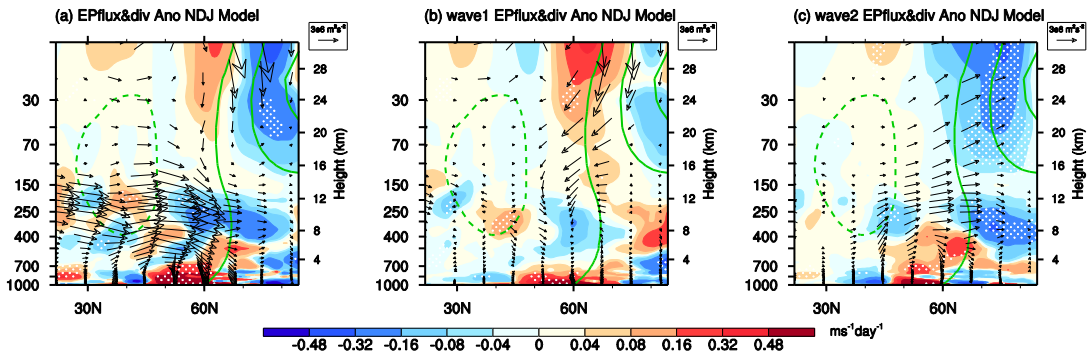

Figure S4 (a) Simulated early winter zonal mean EP flux (vector, unit: $m^2\ s^{-2}$), EP flux divergence (shading, unit: $m\ s^{-1}\ day^{-1}$) and geopotential height anomalies (green contour; interval: -10, 10, 30, 50 m). (b), (c) same as (a), but for the zonal mean EP flux and EP flux divergence anomaly of planetary wave 1 and 2, respectively. Dots for shadings indicate the 90% confidence level. Vectors only depict the part exceeding 10^5 $m^2\ s^{-2}$.

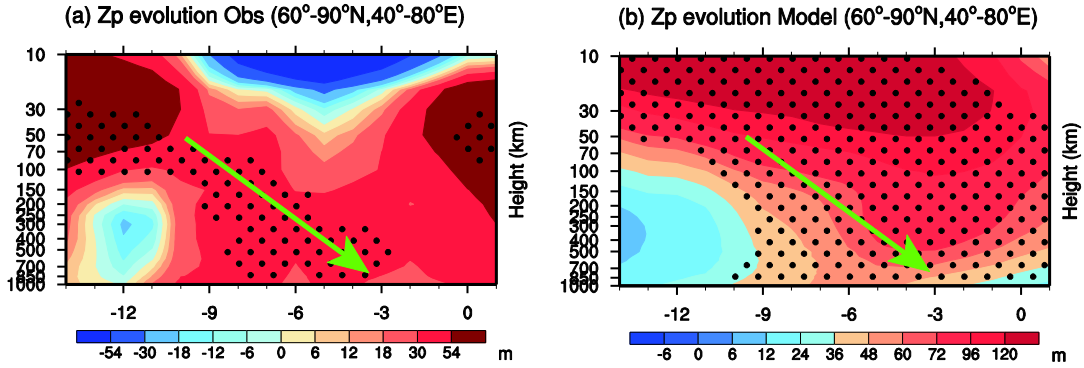

Figure S5 Time-height cross sections from day -14 to day 1 of (a) area-mean detrended geopotential height anomalies (shading; unit: m) over the Ural Mountains (60°-90°N, 40-80°E) during six low EsCB sea ice years. (b) same as (a), but for simulated results. Dots for shadings indicate the 90% confidence level.

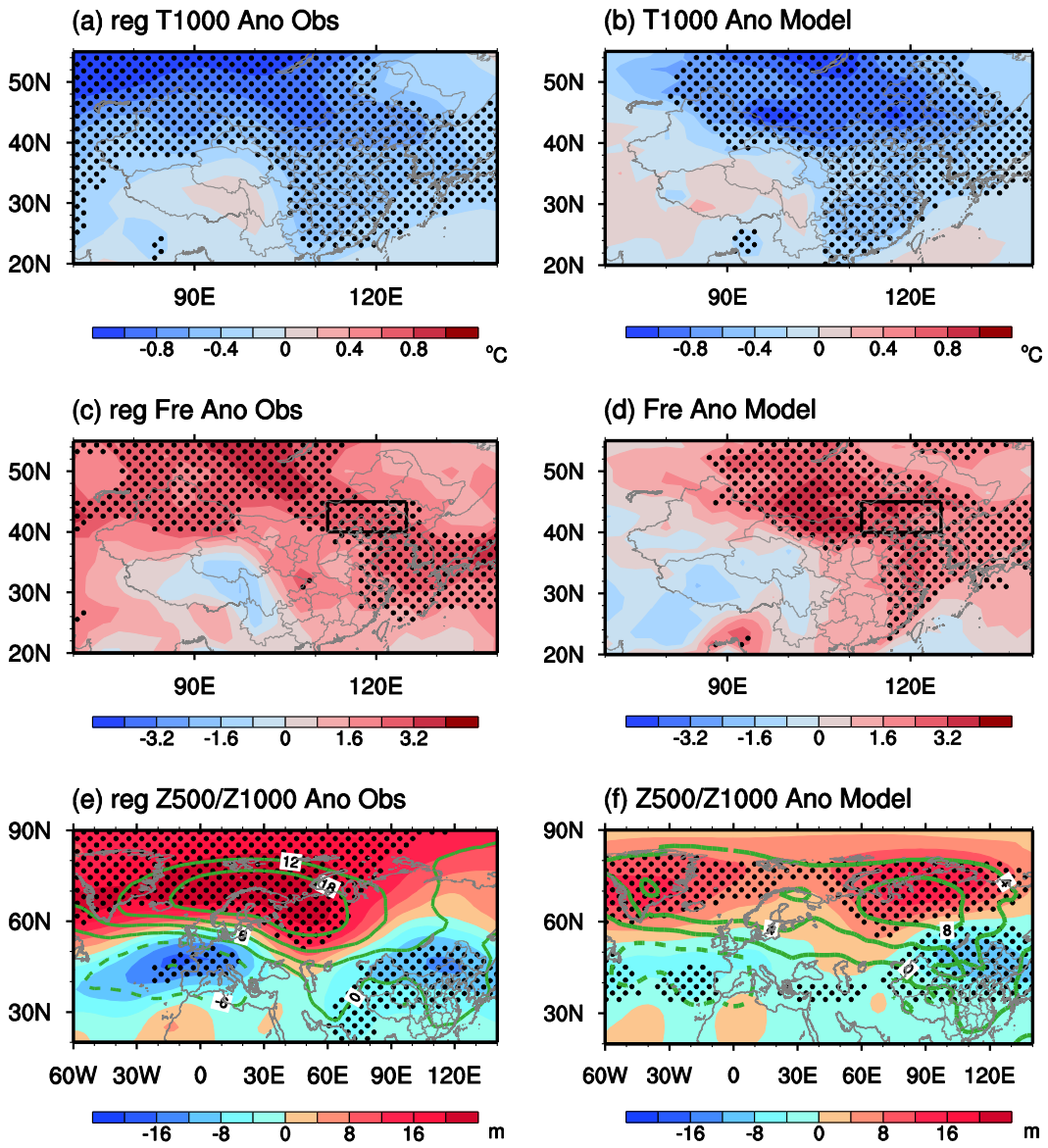

Figure S6 Regressed (a) 1000hPa air temperature (shading, unit: ℃), (c) extreme low temperature frequency, and (e) 1000 (contour, unit: m) and 500 hPa (shading, unit: m) geopotential height anomalies on normalized detrended autumn (September-October) BK (70.5°N–80.5°N, 40.5°E–134.5°E) index (Ding et al. 2021) during 1979/80-1999/00. (b), (d), (f) same as (a), (c), (e), but for simulated results with 100 members forced by composite detrended Arctic SIC with the detrended BK index greater than 0.8σ (low sea ice: 1983, 1984, 1985, 1995, 2009, 2011, 2018). Black dots indicate 90% confidence level.

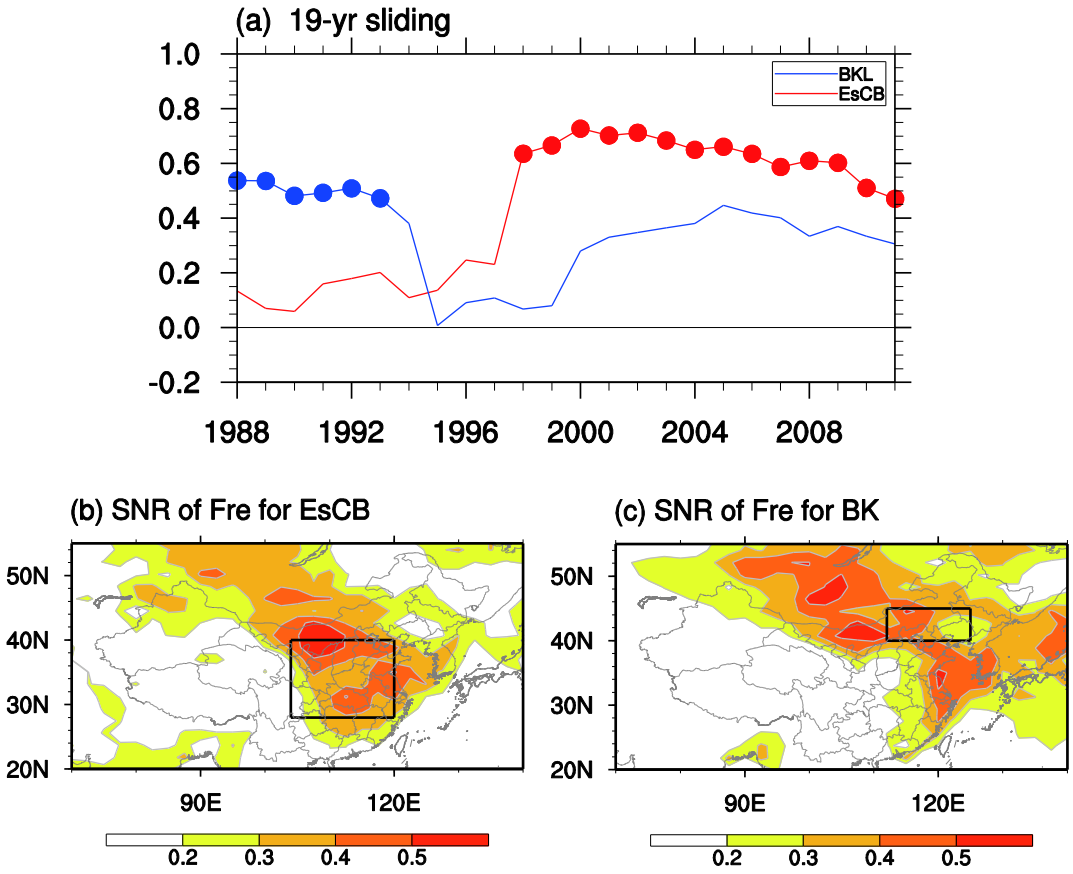

Figure S7 (a) Sliding correlation coefficients between autumn detrended EsCB (BKL) index and winter detrended extreme low temperature frequency over western-central (northwestern) China with a 19-year window. Dots indicate 95% confidence level. (b) Signal-to-noise ratio (SNR) is defined as the frequency change of extreme low temperature induced by EsCB sea ice forcing divided by the model internal variability (standard deviation in control experiments). (c) same as (b), but for BK sea ice loss.

Table S1 The beginning dates and accumulative days for 12 extreme low temperature events in the observation

Year	Beginning date for each event	Days
1980	January 10, January 29	1, 12
1981	December 1	5
1982	January 16	2
1990	December 1	3
2008	January 12, December 4, December 21	36, 2, 3
2009	January 11, February 25	3, 3
2012	December 22	10
2013	February 7	3